Applied Catalysis B: Environmental 125 (2012) 398–408

Contents lists available at SciVerse ScienceDirect

Applied Catalysis B: Environmental

journal homepage: www.elsevier.com/locate/apcatb

NO oxidation over nitrogen doped carbon xerogels

Juliana P.S. Sousa, Manuel F.R. Pereira, José L. Figueiredo*

Laboratório de Catálise e Materiais (LCM), Laboratório Associado LSRE/LCM, Departamento de Engenharia Química, Faculdade de Engenharia, Universidade do Porto, 4200-465 Porto, Portugal

ARTICLE INFO

Article history:
Received 12 March 2012
Received in revised form 6 June 2012
Accepted 12 June 2012
Available online 21 June 2012

Keywords:
NO oxidation
Nitrogen-doping
Carbon xerogels
Carbon catalysts
NO_x abatement

ABSTRACT

Carbon xerogels were prepared from a nitrogen-containing polymer precursor, using melamine and urea as nitrogen sources incorporated into the polymer matrix, by the sol–gel process. Materials with different contents of nitrogen were obtained and used as catalysts for NO oxidation at room temperature. The NO conversions obtained with nitrogen doped carbon xerogels were quite high, showing that carbon xerogels are efficient catalysts for NO oxidation. A maximum of 88% conversion for NO was obtained at NO initial concentration of 1000 ppm and 20% of O_2. The presence of nitrogen-containing surface groups was shown to favour the oxidation of NO to NO_2. The catalytic activity of the catalysts is maintained in consecutive runs.

1. Introduction

NO_x are considered primary atmospheric pollutants, since they are responsible for a wide range of environmental problems like photochemical smog, acid rain, tropospheric ozone and ozone layer depletion [1]. Furthermore, they cause serious health problems in humans [2].

The most popular NO_x abatement technology is selective catalytic reduction (SCR) with ammonia, used mainly to reduce emissions from combustion power plants, but this process has several drawbacks, such as high reaction temperatures (>300 °C) and un-reacted reducing agents [3].

Development of new technologies and improvement of currently used methods are necessary [4], in face of rising restrictions regarding NO_x emissions which are being imposed by the Gothenburg and Kyoto protocols.

The catalytic oxidation of NO to NO_2 at ambient temperature appears to be a promising route for the control of NO emissions, since NO_2 can be subsequently removed by absorbing it in water [5–8].

Carbon xerogels are novel porous carbon materials that have received considerable attention in the literature [9–11]. These materials can be obtained from the carbonization of organic xerogels, which are prepared by sol–gel polycondensation of certain monomers, such as resorcinol and formaldehyde, following Pekala's method [12]. A polycondensation reaction takes place between resorcinol and formaldehyde, yielding a three-dimensional polymer matrix, the RF hydrogel. After solvent exchange and drying, followed by carbonization, a carbon xerogel can be obtained. Subsequent activation can be used to modify the surface properties of the materials [13].

Carbon xerogels can be prepared with other monomer combinations, such as melamine/formaldehyde/resorcinol, phenol/furfural, urea/formaldehyde/resorcinol or polyurethane [14]. If nitrogen containing precursors (melamine and urea) are used, carbon xerogels enriched with non-reactive nitrogen located in the graphene sheets can be obtained [15,16]. Nitrogen doping has been applied to conventional carbon materials, such as activated carbons [17–24].

The oxidation of NO with activated carbons and with activated carbon fibres has been studied by Guo et al. [25], Adapa et al. [26] and Mochida et al. [6,7]. Since the reaction between NO and the carbon materials is a heterogeneous reaction, the surface chemistry of the carbons has large effects on their reactivity. The introduction of nitrogen groups on carbon materials increases the electron density in the basal planes and induces surface basicity, thereby enhancing their catalytic activity for redox reactions [27,28]. Surface nitrogen groups have also been reported to induce the formation of superoxide ions, O_2^- [28,29]. Matzner and Boehm [30] studied the reduction of NO with activated carbons of different nitrogen contents, and observed that the incorporated nitrogen enhanced the reduction activity.

In the present study, urea and melamine were used as precursors to prepare nitrogen-doped carbon xerogels, which were subsequently tested as catalysts for the oxidation of NO.

* Corresponding author. Tel.: +351 22 508 1663; fax: +351 22 508 1449.
E-mail addresses: juliana.sousa@fe.up.pt (J.P.S. Sousa), fpereira@fe.up.pt (M.F.R. Pereira), jlfig@fe.up.pt (J.L. Figueiredo).

0926-3373/$ – see front matter © 2012 Elsevier B.V. All rights reserved.
http://dx.doi.org/10.1016/j.apcatb.2012.06.009

2. Experimental

2.1. Synthesis of nitrogen doped carbon xerogels

Carbon xerogels with nitrogen were prepared as follows: 15 g of resorcinol were added to 3 g of melamine (4 g of urea) in 18 mL of distilled water. The solution was heated to 90 °C under stirring until the melamine (urea) was completely dissolved. Then, it was cooled to room temperature and 20 mL of formaldehyde were added. The pH was adjusted to 5.3 (6.0 and 6.9) with a 2 M NaOH solution. The gelation was accomplished in a water bath at 85 °C for 3 days. The dried gel was carbonized under nitrogen flow (100 $cm^3\ min^{-1}$) at 500 °C (700 °C and 900 °C). The materials were named as CXM or CXU when the precursor used was respectively melamine or urea, followed by the pH value and temperature of carbonization.

2.2. Oxidation of NO

Oxidation of NO on carbon xerogels was carried out in a fixed bed U-shaped flow type reactor. The sample weight, catalyst size, the flow rate, the O_2 concentration, the NO concentration in He and the reaction temperature were 0.2 g, 0.3–0.2 mm, 100 $cm^3\ min^{-1}$, 20%, 1000 ppm, and 25 °C, respectively.

The concentrations of NO and NO_2 at the outlet of the reactor were measured continuously by a high level NO_x analyser (Model 42i-HL Thermo Scientific).

2.3. TPD analyses of adsorbed NO and NO_2

NO and NO_2 adsorbed during the oxidation of NO were determined by temperature programmed desorption. The experiments were conducted over the samples used in the oxidation of 1000 ppm NO with 20% O_2 at room temperature. The samples were heated at 5 °C min^{-1} to 560 °C under He flow, the amounts of NO and NO_2 desorbed being measured by the NO_x analyser.

2.4. Catalyst characterization

2.4.1. Textural characterization

The textural characterization of the carbon materials was based on the N_2 adsorption–desorption isotherms, determined at −196 °C with a Quantachorome Nova 4200e apparatus. The micropore volume (V_{micro}) and mesopore surface area (S_{meso}) were calculated by the *t*-method. The thickness (*t*) of the film adsorbed in multilayers was calculated using the standard isotherm for Carbon Black, given by equation:

$$t_{CB}(\text{Å}) = 0.88\left(\frac{P}{P_0}\right)^2 + 6.45\left(\frac{P}{P_0}\right) + 2.98$$

2.4.2. Surface chemistry characterization

Temperature programmed desorption (TPD) analyses were carried out with an Altamira Instruments AMI-200 apparatus. The amounts of CO and CO_2 released from the decomposition of the surface oxygenated groups were analysed with a mass spectrometer Dymaxion 200 amu, Ametek. The mass numbers (m/e) monitored for all samples were: 2(H_2), 16(O_2), 18(H_2O), 28(CO), 30(NO) and 44(CO_2) [31].

The pH at the point of zero charge (pH_{pzc}) was determined as follows: The pH of a solution of 0.01 M NaCl was adjusted between 2 and 12 by adding either NaOH or HCl. The samples (0.05 g) were added to 20 mL of the solution. After 48 h, the final pH was recorded. A blank experiment (without the carbon material) was carried out in order to subtract the variation of pH caused by the effect of CO_2 present in the head space.

The plots of final pH *vs.* initial pH were used to determine the points at which initial pH and final pH values were equal. This was taken as the pH_{pzc} of the carbon [32].

The carbon, hydrogen and nitrogen contents of nitrogen doped carbon xerogels (in dry basis) were determined using an EA 1108 Elemental Analyser from Carlo Erba instruments.

XPS measurements were made at CEMUP (Centro de Materiais da Universidade do Porto) with a VG Scientific ESCALAB 200A spectrometer, equipped with a Mg Kα X-ray source ($h\upsilon$ = 1253.6 eV). Survey and multiregion spectra were recorded at C_{1s}, O_{1s}, and N_{1s} photoelectron peaks. The internal standard peak for determining binding energies (BEs) was that of carbon C_{1s} (285.0 eV).

3. Results and discussion

3.1. Textural properties of nitrogen doped carbon xerogels

3.1.1. Nitrogen adsorption–desorption isotherms of N-doped carbon xerogels

The textural properties of the prepared nitrogen doped carbon xerogels are strongly affected by the pH of the preparation solution, precursor used and temperature of carbonization. Table 1 shows the textural parameters for all carbon xerogels studied.

In the case of carbon xerogels prepared with melamine, the N_2 adsorption isotherms evolve from type IV to type I when pH increases from 5.3 to 6.9. Specific surface areas, S_{BET}, vary from 19 $m^2\ g^{-1}$ (pH = 6.0) to 630 $m^2\ g^{-1}$ (pH = 5.3). The micropore volumes range from: 0 (pH = 6.0, pH = 6.9) to 0.17 $cm^3\ g^{-1}$ (pH = 5.3).

The carbon xerogels prepared with melamine at pH = 5.3 presented the highest specific surface area and micropore volume for the three carbonization temperatures.

In the case of carbon xerogels prepared with urea, the specific surface areas, S_{BET}, vary from 43 $m^2\ g^{-1}$ (pH = 5.3) to 516 $m^2\ g^{-1}$ (pH = 6.9). The micropore volumes follow the same trend: 0 (pH = 5.3) to 0.12 $cm^3\ g^{-1}$ (pH = 6.9).

This shows that there is a development of the porosity of carbon xerogels prepared with urea as the pH increases. The adsorption isotherms evolve from type I, which are characteristic of microporous materials, to isotherms of type IV, which are characteristic of mesoporous materials.

The highest values of surface area and micropore volume in the carbon xerogels prepared with urea were obtained at pH = 6.9.

Table 1
Textural properties of nitrogen doped carbon xerogels.

Sample	S_{BET} [$m^2\ g^{-1}$]	V_{micro} [$cm^3\ g^{-1}$][a]	S_{meso} [$m^2\ g^{-1}$][a]
CXM-5.3-500 °C	549	0.15	166
CXM-5.3-700 °C	630	0.17	93
CXM-5.3-900 °C	438	0.09	118
CXM-6-500 °C	19	0	19
CXM-6-700 °C	148	0	148
CXM-6-900 °C	135	0.03	64
CXM-6.9-500 °C	60	0	60
CXM-6.9-700 °C	287	0.10	35
CXM-6.9-900 °C	331	0.07	156
CXU-5.3-500 °C	43	0	43
CXU-5.3-700 °C	435	0.09	87
CXU-5.3-900 °C	221	0.06	69
CXU-6-500 °C	77	0	77
CXU-6-700 °C	432	0.08	173
CXU-6-900 °C	110	0.01	92
CXU-6.9-500 °C	516	0.11	256
CXU-6.9-700 °C	461	0.12	122
CXU-6.9-900 °C	460	0.07	269

[a] Micropore volume (V_{micro}) and mesopore surface area (S_{meso}) calculated by the *t*-method.

Table 2
Amount of nitrogen determined by elemental analysis and by XPS; binding energies and relative surface concentrations of nitrogen species obtained by fitting the N 1s core level XPS spectra.

Sample	N[a]	N_{XPS}[b]	N6 groups		N5 groups		N-Q groups	
	w%	w%	B.E. (eV)	w%	B.E. (eV)	w%	B.E. (eV)	w%
CXM-5.3-500 °C	5.3	4.5	398.9	2.3	400.9	1.3	401.7	1.0
CXM-5.3-700 °C	4.0	2.8	398.8	1.4	–	–	401.1	1.3
CXM-5.3-900 °C	3.7	2.8	398.5	1.0	–	–	401.0	1.8
CXM-6-500 °C	4.5	3.7	398.6	2.1	400.1	1.6	–	–
CXM-6-700 °C	4.4	2.6	398.7	1.2	400.9	1.4	–	–
CXM-6-900 °C	3.8	2.2	398.4	0.9	400.5	0.6	401.5	0.7
CXM-6.9-500 °C	5.1	4.5	398.6	2.7	400.4	1.7	–	–
CXM-6.9-700 °C	4.0	3.8	398.6	1.6	400.9	2.2	–	–
CXM-6.9-900 °C	3.6	3.2	398.8	1.4	400.9	0.9	401.9	1.0
CXU-5.3-500 °C	2.8	2.4	398.9	1.5	400.3	0.9	–	–
CXU-5.3-700 °C	2.4	1.9	398.7	0.9	–	–	401.0	1.0
CXU-5.3-900 °C	2.0	2.0	398.5	0.6	–	–	401.1	1.4
CXU-6-500 °C	2.6	2.0	398.7	1.2	400.5	0.8	–	–
CXU-6-700 °C	2.5	2.1	398.4	0.8	400.2	0.6	401.4	0.7
CXU-6-900 °C	2.4	2.0	398.7	1.0	–	–	401.2	1.1
CXU-6.9-500 °C	3.1	2.7	398.9	1.7	400.6	1.0	–	–
CXU-6.9-700 °C	2.9	2.5	398.8	0.9	400.7	0.6	401.7	1.1
CXU-6.9-900 °C	2.7	1.7	398.3	0.7	–	–	401.3	1.0

[a] Nitrogen content determined by elemental analysis.
[b] Nitrogen content determined by XPS.

This means that the reaction between resorcinol, formaldehyde and urea is favourable when using a high synthesis pH.

As one can see in Table 1, the carbon xerogels prepared with melamine present the highest values of surface area. By increasing the synthesis pH the surface area and pore volume of these carbon xerogels decrease.

A high pH in the initial solution produces pores with a structure that does not stand the conditions of drying and carbonization, leading to the nanostructure collapse and to non-porous carbon xerogels. On the other hand, a low pH in the initial solution produces materials with a strong structure, so that the texture remains intact even after treatment at high temperatures.

The specific surface area and micropore volume increase with the pyrolysis temperature, as long as the latter does not exceed 700 °C. Lin and Ritter [33] observed that the micropore volumes decrease due to densification when the carbon xerogels are carbonized above 750 °C, most likely as a result of C—C bond formation at the expense of C—H bond breakage.

3.2. Chemical properties of nitrogen doped carbon xerogels

3.2.1. Nitrogen content

The nitrogen contents obtained by elemental analysis and by XPS measurements are summarized in Table 2.

As expected, the bulk nitrogen content is larger for the carbon xerogels prepared with melamine (5.3–3.6%), compared to the carbon xerogels prepared with urea (3.1–2.0%). This result can be attributed to the fact that melamine contains a larger percentage of nitrogen in its structure than urea (67% *vs.* 47%) [27].

The nitrogen content decreases with the increase of carbonization temperature, but large amounts of nitrogen are still present in the materials even after carbonization at 900 °C. The nitrogen groups introduced with urea are thermally more stable than those introduced with melamine, because the loss of nitrogen is much lower upon increasing the carbonization temperature.

The mechanism of formation of carbon xerogels involves aromatic electrophilic substitution, followed by condensation reactions that lead to crosslinking [34]. The condensation reaction of melamine with formaldehyde is similar to that between urea and formaldehyde. However, the addition of formaldehyde to melamine occurs more easily and completely than its addition to urea. The amino group in melamine easily accepts up to two molecules of formaldehyde. Thus, the complete methylolation of melamine is possible, whereas it is not possible with urea [35]. This means that the major amount of nitrogen is found in the matrix of carbon xerogels when melamine is utilized as nitrogen precursor (major differences between nitrogen content determined by elemental analysis and by XPS), while the nitrogen groups are found mainly on the surface when urea is used (similar nitrogen contents determined by elemental analysis and XPS).

The amount of nitrogen determined by elemental analysis is larger than by XPS, which means that most of the nitrogen is bonded to the carbon matrix.

Thus, N-doped carbon xerogels with a wide variety of N functionalities and contents can be obtained, depending on the N-containing organic monomer and carbonization temperature used.

Fig. 1 shows the deconvoluted XPS N 1s spectra of the nitrogen doped carbon xerogels prepared with melamine and with urea.

Three different BE regions were identified in the N 1s core level spectra of carbon materials: the first region, between 398.0 and 398.9 eV, is usually assigned to pyridine-like N atoms [35–38], which contribute to the π system with one p-electron (denoted as N6). The pyridine-like N-atom is sp^2-hybridized, with the ion-pair electrons in the sp^2 hybrid orbital that does not participate in the π-system, and hence appears in the XPS spectrum at lower BE.

The region between 400.0 and 400.9 eV corresponds to N atoms in a pyrrole-like [35–39] configuration (denoted as N5), donating two π-electrons to the π-system, as is the case for both pyrrole and pyridone functionalities. The pyridone species is a tautomeric form of a lactam, and is represented as a pyridine species with a hydroxyl group in α-position to the N atom in the aromatic ring. The BE region around 401.1 ± 0.8 [36–40] is usually assigned to any form of quaternary nitrogen (NQ). This component is also assigned to the so-called substitutional "graphitic" nitrogen. Substitutional N refers to N substituting a C atom in the graphitic structure, in which nitrogen forms three σ-bonds with neighbouring C or H atoms and contributes with two electrons to the π-system.

The amounts of different types of N-species created on the carbon xerogels were calculated from the deconvoluted N 1s spectra (Table 2).

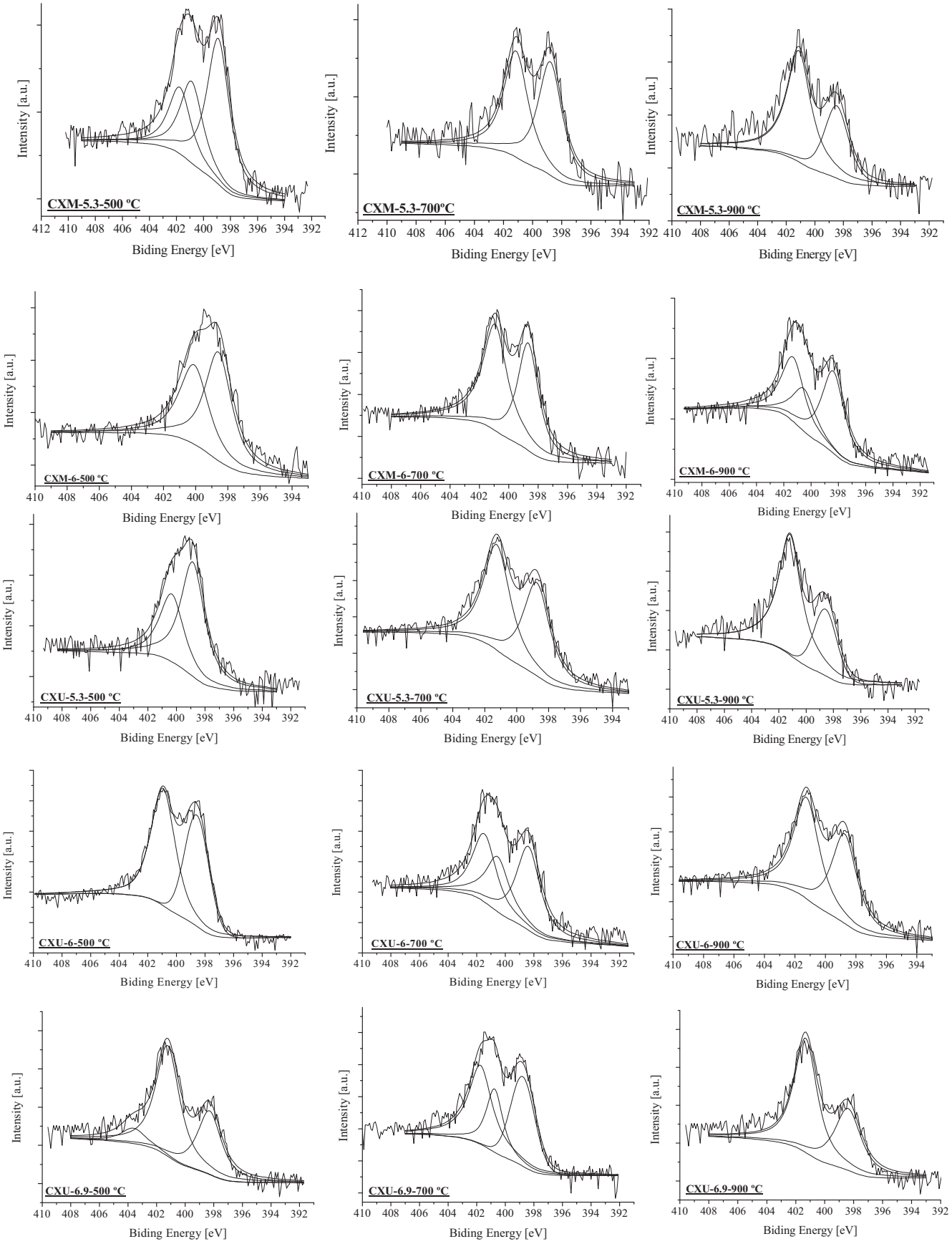

Fig. 1. N1s XPS spectra for all carbon xerogels studied.

Table 3
Amounts of CO and CO_2 obtained from the TPD spectra and pH_{pzc} values of nitrogen doped carbon xerogels.

Sample	pH_{pzc}	CO [μmol g^{-1}][a]	CO_2 [μmol g^{-1}][a]	Sample	pH_{pzc}	CO [μmol g^{-1}][a]	CO_2 [μmol g^{-1}][a]
CXM-5.3-500 °C	6.8	11,000	2595	CXM-6.9-900 °C	7.6	395	169
CXM-5.3-700 °C	7.1	1880	1046	CXU-5.3-500 °C	7.0	3795	709
CXM-5.3-900 °C	8.0	1046	433	CXU-5.3-700 °C	6.9	826	222
CXM-6-500 °C	6.7	3621	633	CXU-5.3-900 °C	7.1	–	–
CXM-6-500 °C-HNO_3	–	2158	2041	CXU-6–500 °C	6.9	3701	321
CXM-6-700 °C	7.2	1346	414	CXU-6-700 °C	7.0	774	288
CXM-6-700 °C-O_2	–	1423	287	CXU-6-900 °C	7.5	221	187
CXM-6-900 °C	7.3	1141	541	CXU-6.9-500 °C	7.1	4177	807
CXM-6.9-500 °C	7.1	2873	556	CXU-6.9-700 °C	7.4	1292	579
CXM-6.9-700 °C	7.1	454	489	CXU-6.9-900 °C	7.1	990	945

[a] Calculated by TPD spectra integration.

The amino groups contained in urea and melamine were lost during carbonization. In the samples carbonized at 500 °C, pyridine is the main peak observed for these carbons, which means that this species is predominantly formed at relatively lower temperatures. As the carbonization temperature increases, the relative intensities of the N5 and N6 components decrease, while that of NQ increases. N5 is converted to N6 at higher carbonization temperatures, which is subsequently converted to NQ, as N atoms are incorporated into the graphene layers [39,41].

The amount of quaternary nitrogen increases with the temperature of carbonization, indicating the chemical change and transformation of nitrogen groups during the heat treatment. The results indicate that pyridine nitrogen has been chemically transformed into nitrogen species with higher binding energies through the condensation reactions occurring during carbonization.

3.2.2. TPD analysis and pH_{pzc}

The TPD experiments were carried out to characterize the oxygen-containing surface groups of different carbon xerogel samples. The oxygenated groups decompose by releasing CO (anhydrides, phenols, carbonyls) or CO_2 (carboxylic acids, anhydrides, lactones) at different temperatures. The total amounts of CO and CO_2 released were calculated from the corresponding TPD spectra and are shown in Table 3.

The carbon xerogels carbonized at 500 °C present large amounts of surface oxygenated groups, which are partially explained by the relatively lower temperature used during preparation. Most of the CO and CO_2 released above 500 °C is still the result of the xerogel matrix carbonization. The amount of oxygen-containing surface groups decreases as the carbonization temperature increases.

All materials obtained have neutral or slightly basic properties, independently of the pH used in their preparation. This can be explained by the presence of nitrogen groups that have basic properties.

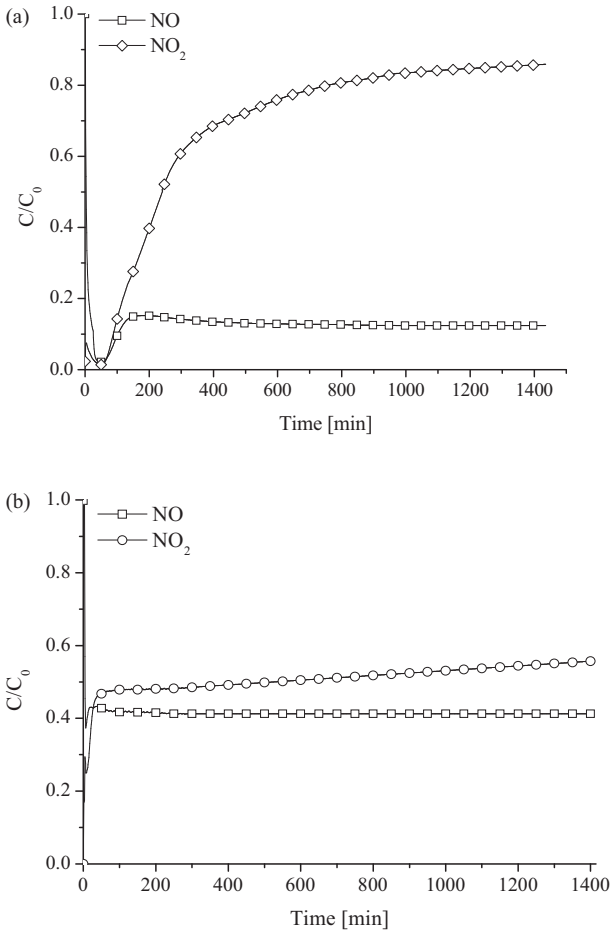

Fig. 2. Breakthrough curves of NO and NO_2 for samples: (a) CXM-5.3-500 °C and (b) CXU-5.3-500 °C.

3.3. Catalytic tests

3.3.1. NO Oxidation over CXM-5.3-500 °C and CXU-5.3-500 °C

Fig. 2 illustrates the breakthrough profiles of NO and NO_2 at room temperature over sample CXM-5.3-500 °C, which is one of the samples that presents the largest NO conversion, and CXU-5.3-500 °C, which presents the worst NO conversion. These experiments were carried out with 1000 ppm of NO and 20% of O_2.

Sample CXM-5.3-500 °C presents a BET surface area of 549 $m^2\ g^{-1}$ and a micropore volume of 0.15 $cm^3\ g^{-1}$, while sample CXU-5.3-500 °C has a surface area of 43 $m^2\ g^{-1}$ and does not have micropores.

No NO_2 is detected at the reactor outlet during the initial stages of the experiment with sample CXM-5.3-500 °C. The NO_2 produced during the first 90 min of reaction is retained on the carbon xerogel. Thereafter, the adsorption sites for NO_2 are saturated, and the concentration of NO_2 in the gas phase increases and reaches a plateau.

The decrease observed in the NO concentration after the peak maximum is ascribed to the rapid increase of NO_2 desorption.

In the case of CXU-5.3-500 °C, NO_2 is detected from the beginning of the reaction, which is justified by the absence of micropores in this sample. Zhang et al. [42] proposed that micropores act as nano-cages for NO/O_2 adsorption, reaction to form NO_2, and chemisorption of NO_2.

The role of carbon xerogels in the present context is of a catalyst, rather than an adsorbent, since the steady-state concentration level of NO remains below that at the inlet, as the carbon xerogel sites are continuously recovered following the desorption of NO_2 from the surface.

The NO conversion is higher with CXM-5.3-500 °C in comparison to sample CXU-5.3-500 °C, because it has a larger amount of nitrogen groups and a higher surface area.

Table 4 summarizes the steady-state conversion of NO into NO_2, the amount of NO_x retained on nitrogen doped carbon xerogels, and the induction periods for NO_2 release. The induction time is the time interval at which the NO_2 produced is completely adsorbed.

The steady-state conversion of NO is defined as $(C_{inlet} - C_{exit,NO})/C_{inlet}$, where C_{inlet} is the inlet concentration of NO and $C_{exit,NO}$ is the outlet concentration of NO in steady state.

A blank experiment was carried out under the same reaction conditions without catalyst, and a NO conversion of 36% was obtained.

Table 4 shows that the NO conversions obtained were quite high, confirming that the carbon xerogels are efficient catalysts for reaction.

The highest conversion of NO obtained was 88%, both for carbon xerogels prepared with melamine (sample CXM-5.3-500 °C) and with urea (sample CXU-6.9-900 °C). However, in general, the highest NO conversions were obtained with the carbon xerogels prepared with melamine, since these materials exhibit the largest surface areas and nitrogen contents.

The conversions of NO obtained with nitrogen doped carbon xerogels are very close to those obtained in the same conditions with activated carbon [24]. In the context of the practical application of NO oxidation, carbon xerogels have the advantage, when compared to activated carbons, that they can be prepared as monoliths.

As shown in Fig. 2(b), NO_2 shows up in the first minutes of reaction for the sample without micropores (CXU-5.3-500 °C). Samples without micropores present the lowest induction times for NO_2 (CXM-6-500 °C, CXM-6-700 °C, CXM-6.9-500 °C, CXU-5.3-500 °C and CXU-6-500 °C), as shown in Table 4.

The samples with micropores have the highest induction time, which means that there is a significant accumulation of adsorbed NO_2. The experiment conducted without catalyst showed that 36% of NO was converted to NO_2, but in experiments with carbon xerogels NO_2 only begins to be released after some time of reaction and with the samples which have the largest micropore volumes the induction times before NO_2 release are large. So it can be concluded that there are at least two types of adsorption sites on the carbon surface, one which adsorbs both NO and NO_2 and another which adsorbs only NO_2 [43].

The amount of NO converted (normalized by the surface area of mesopores) increases with the amount of pyridine and pyrrole groups of the carbon xerogels, as shown in Fig. 3. Only the mesopore surface area was considered, assuming that most of the micropores are not available for reaction at steady state, being blocked by adsorbed NO_x.

The insertion of nitrogen atoms into the graphite lattice lowers the band gap, thus producing higher electron (charge) mobility and lowering the electron work function at the carbon/gas interface

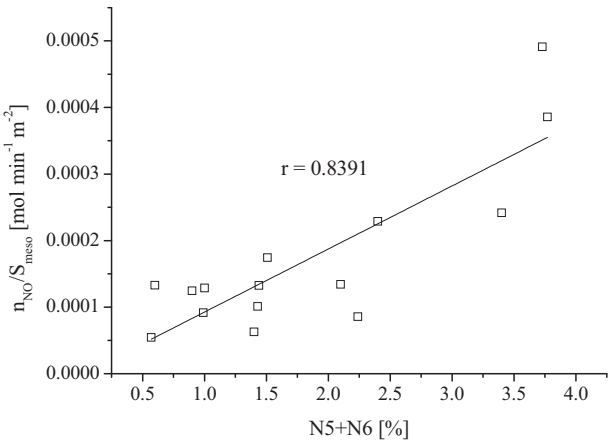

Fig. 3. Rate of NO converted normalized by the surface area of mesopores *vs.* the amount of pyridine and pyrrole groups of the nitrogen doped carbon xerogels.

compared with pure carbons, thus improving the catalytic properties [44–46].

Strelko et al. [46] showed that clusters of only carbon atoms and clusters containing pyridine nitrogen atoms have very high band gap values (ΔE = 4.88 and 4.91 eV, respectively). The band gap energy of the cluster which simulates carbons with pyrrole nitrogen atoms is 2.98 eV, and in the clusters with pyrrole and pyridine nitrogen atoms it is 2.88 eV. These results show that carbons with pyrrole and pyridine nitrogen-containing groups at the edge of graphene layers have the lowest bandgap, thus the highest catalytic activity.

As can be seen in Fig. 3, our results are consistent with these calculations; the nitrogen doped carbon xerogels with larger amounts of N5 and N6 are those with the highest catalytic activity.

In order to evaluate the influence of nitrogen groups on NO oxidation, two experiments were performed with 1000 ppm of NO and 20% of oxygen on a nitrogen doped carbon xerogel and on a carbon xerogel without nitrogen, both having the same surface area (148 $m^2\ g^{-1}$); conversions of 62% and 50% were obtained, respectively. This confirms that the presence of nitrogen enhances the catalytic activity of the carbon xerogels.

3.3.2. Cyclic experiments

Since the stability of a catalyst is an important aspect in the global evaluation of its performance, the most efficient catalyst of this work (CXM-5.3-500 °C) was reused three times in consecutive NO oxidations (Fig. 4). Similar results were obtained in the second and third runs, indicating that the catalytic activity was maintained in consecutive experiments, resulting in NO conversions around 85%. However, a decrease in initial adsorption of NO is observed in the second and third cycles.

In Fig. 4(b) we can observe that NO_2 in the second and third runs shows up in the first minutes of reaction, thus there is no induction time as in the first run; this occurs because the active sites for NO_2

Table 4
Steady-state conversion of NO into NO_2, amount of NO_x ($NO + NO_2$) adsorbed and induction periods for NO_2 release.

Sample	X_{NO} [%]	$t_{Induction,NO_2}$ [min]	$NO_{x,ads}$ [mol g^{-1}]	Sample	X_{NO} [%]	$t_{Induction,NO_2}$ [min]	$NO_{x,ads}$ [mol g^{-1}]
CXM-5.3-500 °C	88	90	1.35	CXU-5.3-500 °C	59	4	0.05
CXM-5.3-700 °C	74	54	0.80	CXU-5.3-700 °C	65	28	0.05
CXM-5.3-900 °C	65	68	0.10	CXU-5.3-900 °C	55	5	0.05
CXM-6-500 °C	56	7	0.02	CXU-6-500 °C	62	3	0.05
CXM-6-700 °C	62	6	0.10	CXU-6-700 °C	65	28	0.10
CXM-6-900 °C	66	56	0.05	CXU-6-900 °C	71	40	1.5
CXM-6.9-500 °C	73	33	0.05	CXU-6.9-500 °C	64	82	0.3
CXM-6.9-700 °C	87	110	1.05	CXU-6.9-700 °C	74	100	0.2
CXM-6.9-900 °C	80	48	0.40	CXU-6.9-900 °C	88	72	0.55

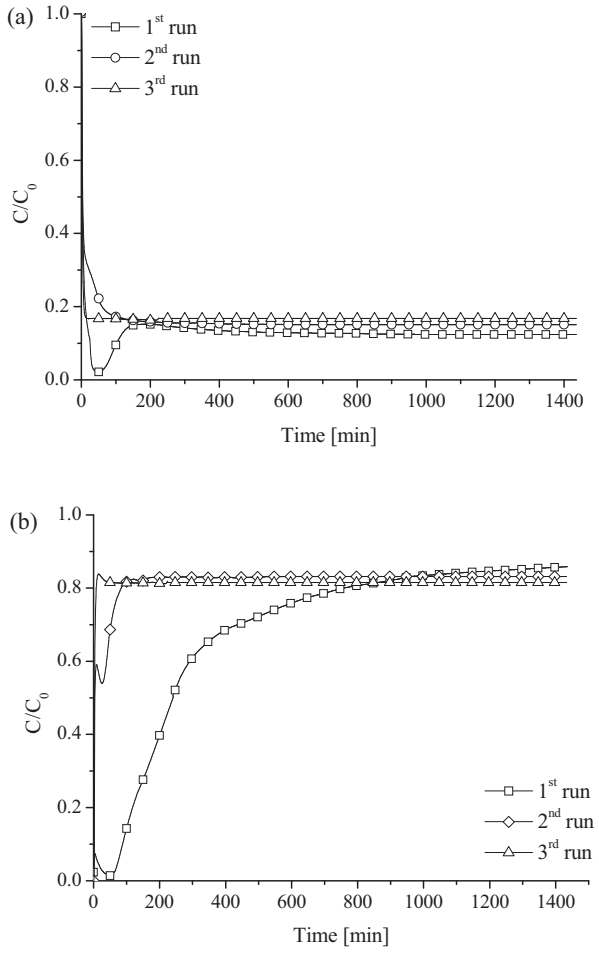

Fig. 4. Evolution of profiles of NO (a) and NO_2 (b) during consecutive reutilization runs of sample CXM-5.3-500 °C.

adsorption are occupied. The amount of NO_2 released in the three runs is very similar, so we can conclude that the catalyst is quite stable under the reaction conditions.

Since the catalyst (CXM-5.3-500 °C) after three experiments presents basically the same NO conversion, NO oxidation by nitrogen doped carbon xerogels seems to be a compatible process for industrial application.

3.3.3. Influence of $C_f(O)$ complexes on the oxidation of NO

It has been demonstrated in the literature that the oxidation of NO is enhanced by the addition of oxygen [24]. Some C(O) complexes are formed on the carbon surface by reaction with oxygen [47]. For a better understanding of the influence of these complexes in the oxidation of NO, additional experiments were carried out, using carbon xerogels modified by oxidative treatments. Sample CXM-6-500 °C was oxidised in the liquid phase with HNO_3 5 M for 6 h (sample CXM-6-500 °C-HNO_3) and sample CXM-6.9-700 °C was oxidized with 5% O_2 at 425 °C for 3 h (sample CXM-6.9-700 °C-O_2).

Compared to the untreated materials, an increase in the surface area was observed for the samples oxidized with nitric acid (S_{BET}: 64 $m^2\ g^{-1}$) and with 5% O_2 (S_{BET}: 668 $m^2\ g^{-1}$). The development of porosity during the oxidative treatments is expected, due to the widening of existing pores and/or creation of new pores [48].

These samples were characterized by TPD, showing that the nitric acid treatment introduces mainly carboxylic acid groups on the surface, while the oxygen treatment introduces essentially CO-releasing groups (phenol and carbonyl-quinones) which have a neutral/basic character [31].

The oxidation of NO on the modified samples was carried out with 1000 ppm of NO and 20% O_2 at room temperature. NO conversions of 54% and 76% were obtained respectively with samples CXM-6-500 °C-HNO_3 and CXM-6.9-700 °C-O_2. These values are lower than those obtained with the original materials (56% and 87%, respectively). This suggests that the oxidative modifications, which produced a carbon surface largely covered by C (O) complexes, inhibits the reaction of NO with carbon at low temperatures.

Richter [49] proposed that a more oxidized surface, formed by the reaction between gas phase O_2 and the activated carbon, serves as active sites for NO adsorption. However, the observations in the present paper and in selected literature [50,51] clearly show that when the carbon surface is saturated with oxygen, the reaction of NO with carbon at low temperatures ceases.

3.4. Kinetic and mechanistic study of NO oxidation

Knowledge of reaction mechanism is essential for the development of the kinetic model, but there is little information available in the literature about the interaction between NO and the carbon surface.

3.4.1. Mechanism

The oxidation of NO into NO_2 may appear simple, as only one oxygen atom is stoichiometrically added to NO. However, the detailed process of NO oxidation and the factors that control it are still under discussion. Ahmed et al. [52] suggested that NO is oxidized by oxygen to NO_2 in the gas phase and then NO_2 is adsorbed on the carbon surface. But the result of the homogeneous oxidation of NO in gas phase is too slow to account for the observed NO oxidation with carbon xerogels. Mochida et al. [5] proposed that NO is adsorbed, oxidized into adsorbed NO_2, which desorbs as the product NO_2. Since NO is a supercritical gas at ambient temperature, very little NO can be physically adsorbed.

Zhang et al. [42] proposed that NO oxidation on activated carbon is a micropore filling process with NO as the adsorbed species. In other words, the narrow micropores in activated carbons act as a nano-catalytic reactor for NO oxidation.

Rathore et al. [53] defended that the gaseous NO and O_2 adsorb on the active sites of activated carbon fibre, followed by oxidation of NO into adsorbed NO_2. The NO_2 adsorbed may further react and form various adsorbed intermediates such as NO_3 and NO-NO_3. Finally, NO-NO_3 is desorbed into NO_2, thereby releasing the sites for the subsequent adsorption of the reactants.

It has also been proposed by other groups that NO reacts with the surface oxygen atoms present on activated carbons [50,51], but this argument is difficult to reconcile with the results obtained here, where the presence of oxygen groups on the surface of carbon xerogels decreases NO conversion.

Based on previous experimental results [24] and some literature [7,43,54], we assume that oxygen is first adsorbed on the surface of carbon xerogels (dissociative adsorption of oxygen, Eq. (1)), and then NO reacts with the adsorbed oxygen to form chemisorbed NO_2 (surface reaction of $NO_{(g)}$ with the adsorbed oxygen, Eq. (3)) which desorbs as the product NO_2 (Eq. (4)). Besides these steps, our mechanism also includes an equation which represents NO adsorption on carbon xerogels (Eq. (2)), and another which represents the reaction between adsorbed NO and adsorbed O_2 (Eq. (3)). We have observed that NO is not adsorbed onto the carbon xerogel in the absence of oxygen (Fig. 5), so it can be concluded that the nitrogen groups incorporated as N5 or N6 do not activate the NO molecule. A different situation has been reported when amine or amide groups are introduced into the surface, which can interact with NO and NO_2 [55]. To establish the mechanism, we considered that the active sites for oxygen chemisorption are unsaturated carbon atoms at the edges of the graphene layers or on basal plane defects, NO from

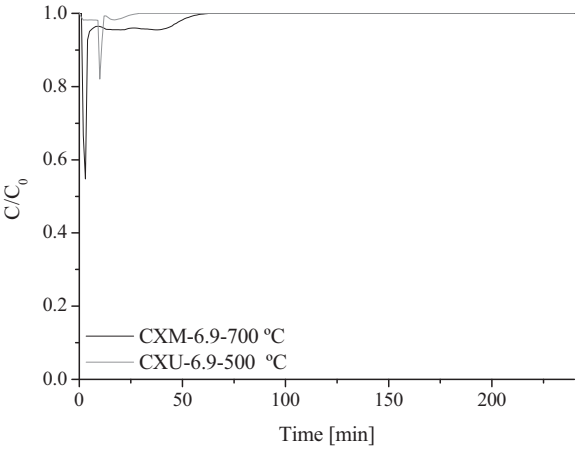

Fig. 5. Adsorption of NO at 25 °C on samples CXM-6.9-700 °C and CXU-6.9-500 °C.

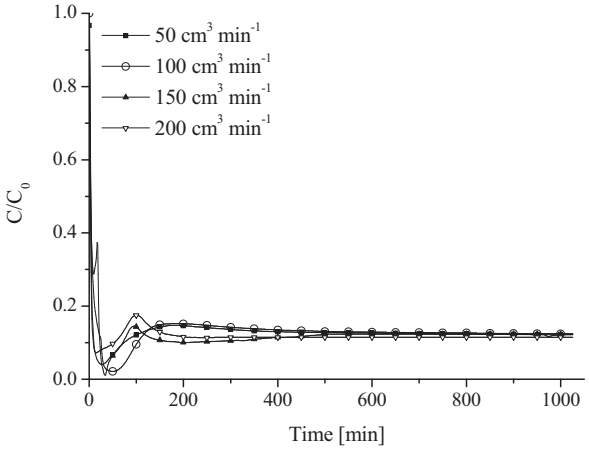

Fig. 6. Profiles of NO obtained with sample CXM-5.3-500 °C for the different flow rates and varying proportionally the mass of catalyst to maintain the contact time constant.

the gas phase reacting with chemisorbed oxygen. Hence, Eqs. (2) and (3) were neglected.

$$O_2 + 2C_f() \leftrightarrow 2C(O) \qquad K_1 \tag{1}$$

$$NO_{(g)} + C_f() \leftrightarrow C(NO) \qquad K_2 \tag{2}$$

$$C(NO) + C(O) \leftrightarrow C(NO_2) + C_f() \qquad K_3 \tag{3}$$

$$NO_{(g)} + C(O) \leftrightarrow C(NO_2) \qquad K_4 \tag{4}$$

$$C(NO_2) \leftrightarrow C_f() + NO_{2(g)} \qquad k_d \tag{5}$$

Here, K_i represents an equilibrium constant and k_i a rate constant. The symbol $C_f()$ represents a free active centre of carbon and the symbols C(NO), C(O) and $C(NO_2)$ represent the active centres occupied, respectively, with NO, O and NO_2.

When the catalyst bed begins to saturate with NO_2, a large increase in the NO outlet concentration was observed, reaching a maximum value. At the same time, breakthrough of NO_2 occurs, which results in the vacant sites. Adsorption of O_2 on the new vacant sites may proceed only when NO_2 is desorbed to release these sites. Therefore, NO_2 desorption (Reaction 5) is the rate-limiting step, as proposed by Adapa et al. [26]. Then:

$$r = k_d[C(NO_2)] \tag{6}$$

The rate equation has an unknown variable, $[C(NO_2)]$, which must be expressed in terms of measurable variables and equilibrium constants. The concentrations of different adsorbed species are obtained as:

$$[C(O)] = K_1^{1/2}[O_2]^{1/2}[C_f()] \tag{7}$$

$$[C(NO_2)] = K_4[NO][C(O)] \tag{8}$$

$$[C(NO_2)] = K_4K_1^{1/2}[O_2]^{1/2}[NO][C_f()] \tag{9}$$

Replacing Eq. (9) in the rate equation, we obtain:

$$r = k_dK_4K_1^{1/2}[O_2]^{1/2}[NO][C_f()] \tag{10}$$

The conservation equation for total number of sites $[C_t]$ may be written as follows:

$$[C_t] = \left[C_f()\right] + [C(O)] + [C(NO_2)] \tag{11}$$

Substituting the expressions written above (Eqs. (7) and (9)) in Eq. (11):

$$[C_t] = \left[C_f()\right] + K_1^{1/2}[O_2]^{1/2}[C_f()] + K_4K_1^{1/2}[O_2]^{1/2}[NO][C_f()] \tag{12}$$

Solving the equation in order to $[C_f()]$:

$$[C_f()] = \frac{[C_t]}{1 + K_1^{1/2}[O_2]^{1/2} + K_4K_1^{1/2}[O_2]^{1/2}[NO]} \tag{13}$$

Substituting Eq. (13) in Eq. (10), we obtain the rate of NO oxidation as:

$$r = \frac{k_dK_4K_1^{1/2}[O_2]^{1/2}[NO][C_t]}{1 + K_1^{1/2}[O_2]^{1/2} + K_4K_1^{1/2}[O_2]^{1/2}[NO]} \tag{14}$$

3.4.2. Kinetic study

3.4.2.1. Preliminary tests. Preliminary experiments were carried out to establish the appropriate experimental conditions to assess the intrinsic kinetic parameters of oxidation of NO.

3.4.2.2. External diffusional limitations. In order to ascertain the possible effect of external diffusional limitations (mass transfer), catalytic tests feeding different mass flow rates and varying proportionally the mass of catalyst to maintain the contact time constant (W/F) were performed.

Fig. 6 represents the profiles of NO obtained with the sample CXM-5.3-500 °C for the different flow rates.

Independently of the flow rate used, the conversion was always the same, so it is possible to conclude that external diffusional limitations are negligible.

3.4.2.3. Internal diffusional limitations. In order to ascertain the effect of internal diffusion limitations, the performance of the catalyst with average particle diameters in the ranges 0.5–0.3 mm and 0.3–0.2 mm was compared. Identical profiles of NO oxidation were obtained, so pore diffusion limitations are negligible.

3.4.2.4. Effect of inlet NO concentration. Experiments with different inlet NO concentrations (250, 500, 750 and 1000 ppm) with sample CXM-5.3-500 °C and with 20% of oxygen were carried out.

The NO conversion increases from 66% to 88% when the NO inlet concentration increases from 250 to 1000 ppm. It appears that NO conversion depends on NO concentration.

Based on the assumptions described, the expression for the rate of NO oxidation can be rewritten in the form:

$$r = \frac{k_{c1}[NO]}{k_{c2} + [NO]k_{c3}} \tag{15}$$

where,

$$k_{c1} = k_dK_4K_1^{1/2}[O_2]^{1/2}[C_t] \tag{16}$$

Table 5
Kinetic parameters obtained for sample CXM-5.3-500 °C.

F_{NO} [mol min^{-1}]	W/F_{NO} [g min mol^{-1}]	xs [%]	k_{c4} [mol L^{-1}]	k_{c5} [g min L^{-1}]
0.0033	60	88	1.13	4.20
0.0050	40	76		
0.0067	30	64		

$$k_{c2} = 1 + K_1^{1/2}[O_2]^{1/2} \quad (17)$$

$$k_{c3} = K_4 K_1^{1/2}[O_2]^{1/2} \quad (18)$$

The reaction rate constants k_{c1}, k_{c2} and k_{c3} are three parameters that have a complex dependency on the concentrations of the reactants.

Simplifying Eq. (15):

$$r = \frac{k_{c4}[NO]}{1 + [NO]k_{c5}} \quad (19)$$

where:

$$k_{c4} = \frac{k_{c1}}{k_{c2}} \quad (20)$$

$$k_{c5} = \frac{k_{c3}}{k_{c2}} \quad (21)$$

A plug-flow tubular reactor was used in the kinetic experiments. Temperature and pressure were assumed constant in the reactor. Taking into account the high dilution of NO, the gas flow rate is constant and:

$$\frac{W}{F_{NO_0}} = \int_0^{xs} \frac{dx}{r} \quad (22)$$

where: W is the mass of catalyst; x is the NO conversion; r is the rate of oxidation of NO; F_{NO_0} is the inlet molar flow rate of NO; x_s is the conversion at the outlet of the reactor.

Expressing the concentration of NO as a function of conversion in Eq. (19):

$$r = \frac{k_{c4}[NO_0](1-x)}{1 + k_{c5}[NO_0](1-x)} \quad (23)$$

Substituting the reaction rate expression in the material balance equation for the reactor:

$$\frac{W}{F_{NO_0}} = \int_0^{xs} \frac{1 + k_{c5}[NO_0](1-x)}{k_{c4}[NO_0](1-x)}\, dx \quad (24)$$

Simplifying:

$$\frac{W}{F_{NO_0}} = \int_0^{xs} \left(\frac{1}{k_{c4}[NO_0](1-x)} + \frac{k_{c5}}{k_{c4}} \right) dx \quad (25)$$

Integrating Eq. (25) between zero and the conversion at the outlet of the reactor (xs):

$$\frac{W}{F_{NO_0}} = \frac{k_{c5}}{k_{c4}} xs - \frac{\ln(1-xs)}{[NO_0]k_{c4}} \quad (26)$$

k_{c4} and k_{c5} can be calculated from a plot of $W/F_{NO_0} xs$ *vs.* $-(\ln(1-xs)/[NO_0]xs)$.

Experiments with sample CXM-5.3-500 °C with 1000 ppm of NO and 20% of oxygen for different contact times were carried out. This sample was chosen because it presented the largest conversion of NO.

Fig. 7 shows the relationship between $W/F_{NO_0} xs$ and $-(\ln(1-xs)/[NO_0]xs)$ A straight line was obtained, allowing the determination of k_{c4} and k_{c5}, which are collected in Table 5.

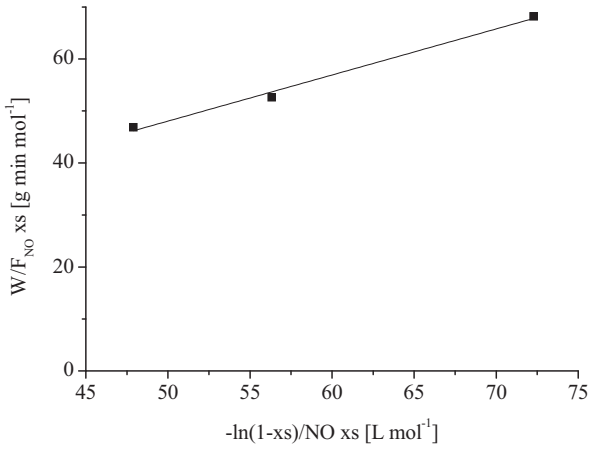

Fig. 7. Plot of $-\ln(1-xs)$/NO *xs vs.* W/F_{NO} *xs*.

3.5. Temperature programmed desorption after NO oxidation on the nitrogen doped carbon xerogels

Fig. 8 illustrates the TPD profiles of NO and NO_2 over the different carbon xerogel samples after reaction with 1000 ppm NO and 20% of O_2. The release of NO and NO_2 was observed in the range of 25–560 °C.

The TPD results show that mainly NO is desorbed between 100 and 300 °C, both for the carbon xerogels prepared with melamine and urea.

A significant amount of desorbed NO was obtained. Nevertheless, in the experiments carried out without oxygen, it was observed that NO practically did not adsorb on the carbon. Fig. 8(b) shows that only a little amount of NO_2 is desorbed, indicating that by heat treatment the NO_2 adsorbed on the surface is reduced, releasing NO. The desorbed NO_2 corresponds to the amount which was adsorbed on the non-reductive sites. The TPD profiles of NO and NO_2 obtained over the nitrogen doped carbon xerogels after reaction are different from those described in the literature with activated carbons [24] or activated carbon fibres [5]. In those cases, mainly NO_2 is obtained in the TPD of the samples analysed after the reaction. Therefore, it may be concluded that carbon xerogels have larger amounts of active sites for the reduction of NO_2 to NO than activated carbons and activated carbon fibres.

Klose and Rincón [56] proposed that NO desorbed between 250 and 300 °C is due to the desorption of $(NO)_2$ dimer. Matzner and Boehm [30] described that the formation of $(NO)_2$ dimer can occur due to the transfer of extra π-electrons of nitrogen groups from the higher energy states to the adsorbed NO molecules.

3.6. Isotherms of sample CXM-5.3-500 °C after NO oxidation

Fig. 9 shows the nitrogen adsorption isotherms at −196 °C on sample CMX-5.3-500 °C after and before reaction. The samples were degassed for 3 h at temperatures of 120 °C and 350 °C.

The isotherms of the sample before and after reaction degassed at 350 °C and the isotherm of the sample before reaction degassed at 120 °C are very similar.

The sample before reaction and degassed at 120 °C presents a slightly lower surface area than the sample degassed at 350 °C due to the presence of some water, that was not completely removed due to the lower degassing temperature.

The sample subjected to NO oxidation and degassed at 120 °C presented a decrease of 82% in the BET surface area and 99% in the micropore volume, which may be explained by pore blockage due to adsorbed NO_2. As noted earlier, large quantities of NO/NO_2 are still being released in the TPD experiments after 120 °C. By heat

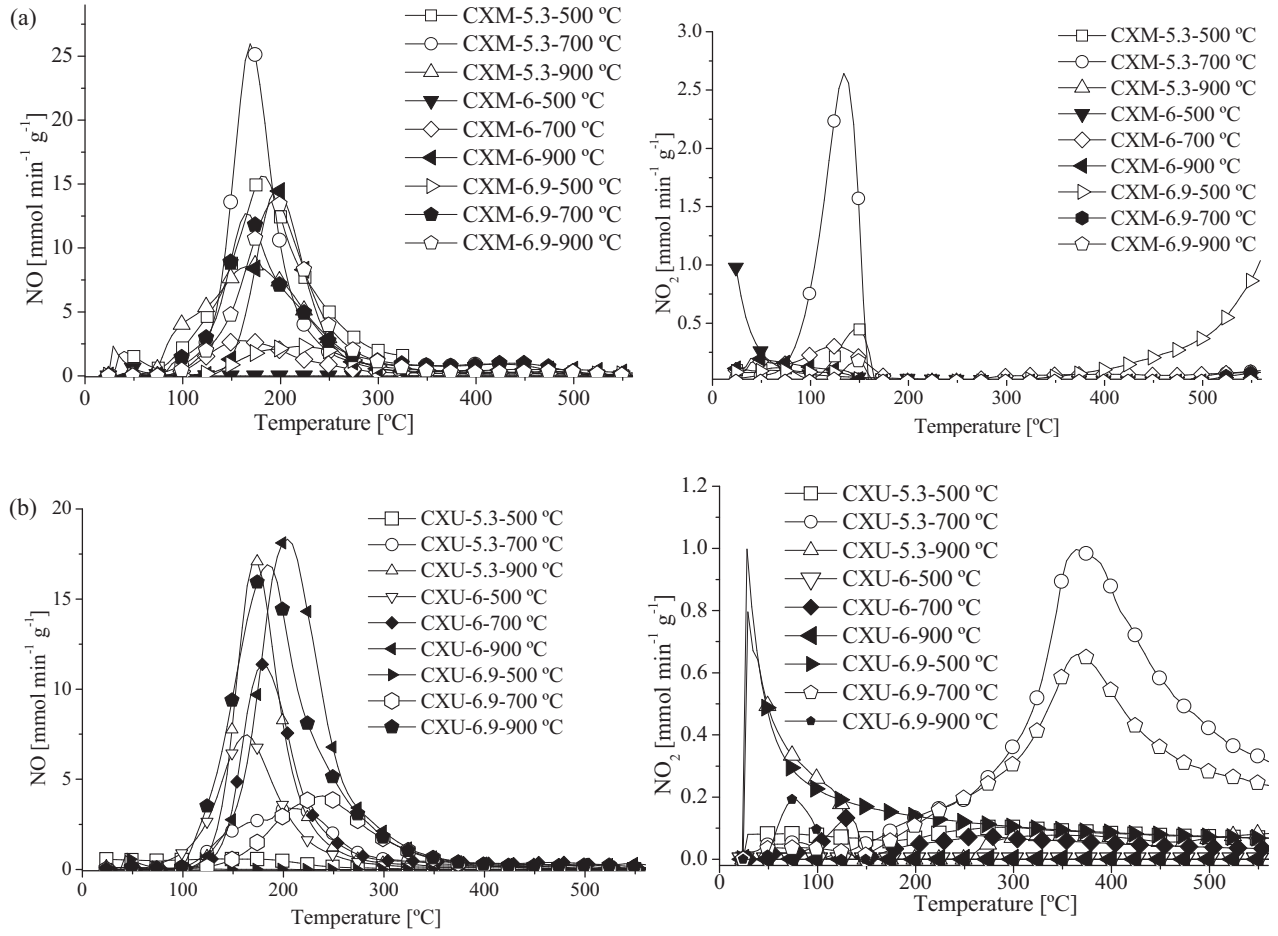

Fig. 8. Desorption profiles for the different samples after reaction with 1000 ppm of NO and 20% O_2: (a) carbon xerogels prepared with melamine and (b) carbon xerogels prepared with urea.

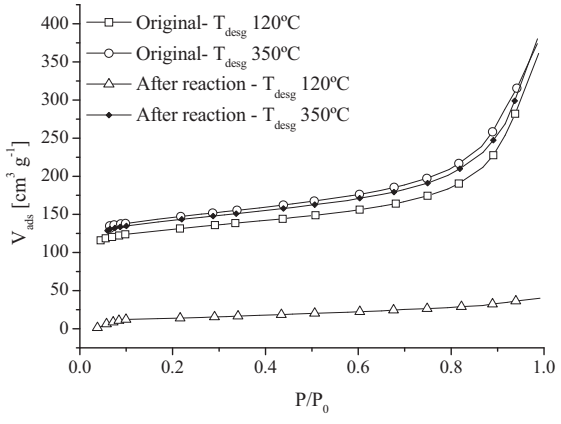

Fig. 9. Nitrogen adsorption isotherms on sample CXM-5.3-500 °C before and after NO oxidation.

treating the sample at 350 °C most of the adsorbed NO_2 is released, and the initial textural properties are recovered.

4. Conclusions

Carbon xerogels containing nitrogen in their structure were prepared by using melamine and urea by the sol–gel process. The textural and chemical properties of the carbon xerogels depend on the pH of preparation, precursor used and carbonization temperature.

The nitrogen doped carbon xerogels are effective catalysts for NO oxidation at room temperature.

The presence of pyridine and pyrrole groups in the carbon materials favours the oxidation of NO to NO_2. The presence of oxygen complexes on the surface of carbon xerogels inhibits NO oxidation.

Acknowledgements

This work was financially supported by Fundação para a Ciência e a Tecnologia (FCT) and FEDER through "Program COMPETE (FCT Pest-C/EQB/LA0020/2011)" and research fellowship SFRH/BD/45720/2008 (JPSS).

References

[1] M. Wojciechowska, S. Lomnicki, Clean Technologies and Environmental Policy 1 (1999) 237–247.
[2] A. Fritz, V. Pitchon, Applied Catalysis B: Environmental 13 (1997) 1–25.
[3] J. Muñiz, G. Marbán, A.B. Fuertes, Applied Catalysis B: Environmental 23 (1999) 25–35.
[4] K. Skalska, J.S. Miller, L. Stanislaw, Science of the Total Enviroment 408 (2010) 3976–3989.
[5] I. Mochida, N. Shirahama, S. Kawano, Y. Korai, A. Yasutake, M. Tanoura, S. Fujii, M. Yoshikawa, Fuel 79 (2000) 1713–1723.
[6] I. Mochida, Y. Kawabuchi, S. Kawano, Y. Matsumura, M. Yoshikawa, Fuel 76 (1997) 543–548.
[7] Y. Kong, C.Y. Cha, Carbon 34 (1996) 1027–1033.
[8] A. Claudino, J.L. Soares, R.F.P.M. Moreira, H.J. José, Carbon 42 (2004) 1483–1490.
[9] F.J. Maldonado-Hódar, M.A. Ferro-García, J. Rivera-Utrilla, C. Moreno-Castilla, Carbon 37 (1999) 1199–1205.
[10] H. Tamon, H. Ishizaka, M. Mikami, M. Okazaki, Carbon 35 (1997) 791–796.
[11] H. Tamon, H. Ishizaka, T. Yamamoto, T. Suzuki, Carbon 37 (1999) 2049–2055.
[12] R.W. Pekala, Journal of Materials Science 24 (1989) 3221–3227.

[13] P.V. Samant, F. Gonçalves, M.M.A. Freitas, M.F.R. Pereira, J.L. Figueiredo, Carbon 42 (2004) 1321–1325.
[14] H.F. Gorgulho, F. Gonçalves, M.F.R. Pereira, J.L. Figueiredo, Carbon 47 (2009) 2032–2039.
[15] K. Jurewicz, R. Pietrzak, P. Nowicki, H. Wachowska, Electrochimica Acta 53 (2008) 5469–5475.
[16] M. Pérez-Cadenas, C. Moreno-Castilla, F. Carrasco-Marín, A.F. Pérez-Cadenas, Langmuir 25 (2008) 466–470.
[17] S. Biniak, G. Szymanski, J. Siedlewski, A. Swiatkowski, Carbon 35 (1997) 1799–1810.
[18] J.P. Boudou, P. Parent, F. Suárez-García, S. Villar-Rodil, A. Martínez-Alonso, J.M.D. Tascón, Carbon 44 (2006) 2452–2462.
[19] A.D. Budaeva, E.V. Zoltoev, Fuel 89 (2010) 2623–2627.
[20] R.J.J. Jansen, H. van Bekkum, Carbon 33 (1995) 1021–1027.
[21] E. Raymundo-Piñero, D. Cazorla-Amorós, A. Linares-Solano, Carbon 41 (2003) 1925–1932.
[22] L. Singoredjo, F. Kapteijn, J.A. Moulijn, J.-M. Martín-Martínez, H.-P. Boehm, Carbon 31 (1993) 213–222.
[23] C.A. Toles, W.E. Marshall, M.M. Johns, Carbon 37 (1999) 1207–1214.
[24] J.P.S. Sousa, M.F.R. Pereira, J.L. Figueiredo, Catalysis Today 176 (1) (2011) 383–387.
[25] Z. Guo, Y. Xie, I. Hong, J. Kim, Energy Conversion and Management 42 (2001) 2005–2018.
[26] S. Adapa, V. Gaur, N. Verma, Chemical Engineering Journal 116 (2006) 25–37.
[27] M. Seredych, D. Hulicova-Jurcakova, G.Q. Lu, T.J. Bandosz, Carbon 46 (2008) 1475–1488.
[28] H.P. Boehm, in: P. Serp, J.L. Figueiredo (Eds.), Carbon Materials for Catalysis, John Wiley & Sons, Hoboken, NJ, 2009, pp. 219–265 (Ch. 7).
[29] B. Stöhr, H.P. Boehm, R. Schlögl, Carbon 29 (1991) 707–720.
[30] S. Matzner, H.P. Boehm, Carbon 36 (1998) 1697–1703.
[31] J.L. Figueiredo, M.F.R. Pereira, M.M.A. Freitas, J.J.M. Órfão, Carbon 37 (1999) 1379–1389.
[32] J. Figueiredo, J. Sousa, C. Orge, M. Pereira, J. Órfão, Adsorption 17 (2011) 431–441.
[33] C. Lin, J.A. Ritter, Carbon 38 (2000) 849–861.
[34] C. Lin, J.A. Ritter, Carbon 35 (1997) 1271–1278.
[35] S. Kim, H.-J. Kim, Bioresource Technology 96 (2005) 1457–1464.
[36] J.P. Boudou, M. Chehimi, E. Broniek, T. Siemieniewska, J. Bimer, Carbon 41 (2003) 1999–2007.
[37] F. Kapteijn, J.A. Moulijn, S. Matzner, H.P. Boehm, Carbon 37 (1999) 1143–1150.
[38] K. Stanczyk, R. Dziembaj, Z. Piwowarska, S. Witkowski, Carbon 33 (1995) 1383–1392.
[39] J.R. Pels, F. Kapteijn, J.A. Moulijn, Q. Zhu, K.M. Thomas, Carbon 33 (1995) 1641–1653.
[40] A.N. Buckley, Fuel Processing Technology 38 (1994) 165–179.
[41] J. Lahaye, G. Nanse, P. Fioux, A. Bagreev, A. Broshnik, V. Strelko, Applied Surface Science 147 (1999) 153–174.
[42] W.J. Zhang, S. Rabiei, A. Bagreev, M.S. Zhuang, F. Rasouli, Applied Catalysis B: Environmental 83 (2008) 63–71.
[43] Z. Zhu, Z. Liu, S. Liu, H. Niu, Fuel 79 (2000) 651–658.
[44] R. Czerw, M. Terrones, J.C. Charlier, X. Blase, B. Foley, R. Kamalakaran, N. Grobert, H. Terrones, D. Tekleab, P.M. Ajayan, W. Blau, M. Rühle, D.L. Carroll, Nano Letters 1 (2001) 457–460.
[45] K. Jurewicz, K. Babeł, R. Pietrzak, S. Delpeux, H. Wachowska, Carbon 44 (2006) 2368–2375.
[46] V.V. Strelko, V.S. Kuts, P.A. Thrower, Carbon 38 (2000) 1499–1503.
[47] Z.G. Zhang, T. Kyotani, A. Tomita, Energy & Fuels 3 (1989) 566–571.
[48] W.M.A.W. Daud, A.H. Houshamnd, Journal of Natural Gas Chemistry 19 (2010) 267–279.
[49] E. Richter, Catalysis Today 7 (1990) 93–112.
[50] Y. Komatsubara, S. Ida, H. Fujitsu, I. Mochida, Fuel 63 (1984) 1738–1742.
[51] K. Kusakabe, M. Kashima, S. Morooka, Y. Kato, Fuel 67 (1988) 714–718.
[52] S.N. Ahmed, R. Baldwin, F. Derbyshire, B. McEnaney, J. Stencel, Fuel 72 (1993) 287–292.
[53] R.S. Rathore, D.K. Srivastava, A.K. Agarwal, N. Verma, Journal of Hazardous Materials 173 (2010) 211–222.
[54] B.R. Stanmore, V. Tschamber, J.F. Brilhac, Fuel 87 (2008) 131–146.
[55] E. Deliyanni, T.J. Bandosz, Langmuir 27 (2011) 1837–1843.
[56] W. Klose, S. Rincón, Fuel 86 (2007) 203–209.